Journal of Thermal Analysis and Calorimetry
https://doi.org/10.1007/s10973-024-13452-6

Mining fan end cooling heat exchanger circuit optimization analysis using micro-unit method

Yongliang Zhang[1] · Zhen Hu[1] · Hongwei Mu[1] · Xilong Zhang[1] · Shouqing Lu[1] · Qinglei Tan[1] · Bing Shao[1]

Received: 27 October 2023 / Accepted: 8 July 2024

Abstract

To address the issue of low efficiency in cooling heat exchangers at the deeper ends of mine fans, we propose a micro-unit approach for arranging the cooling water flow path within the heat exchanger. This method involves subdividing the heat exchanger into micro heat transfer units and determining the heat transfer characteristics of each individual unit through theoretical calculations and software simulations. Utilizing a computer program, these micro units are systematically arranged and combined to exhaust all possible cooling water flow paths. The ultimate objective is to derive the optimal structural arrangement of the cooling water flow path within the heat exchanger, with the goal of achieving the most efficient heat transfer effect. The findings reveal that the optimized structure, obtained through the micro-unit optimization method, achieves an average air outlet temperature of 311.65 K. This temperature is lower than that of the typical current-flow structure (311.88 K) and the typical counter-flow structure (311.68 K), indicating a superior heat transfer effect. Further examination demonstrates that the average air outlet temperature across all counter-flow structures is 311.68 K, which is notably lower than the average air outlet temperature of 311.90 K observed in the current-flow structure. This highlights the enhanced heat transfer effectiveness of the counter-flow structure. This novel method for optimizing the heat exchanger flow path applies the concept of finite element analysis to the optimization process, reducing computational and experimental costs. This approach is significant for improving the efficiency of heat exchangers.

Keywords Mine heat damage · Heat exchanger flow path design · Micro-unit method · Convective heat transfer · Numerical simulation

List of symbols

A_f	Airflow inlet area, m^2
A_{fin}	Fin area, m^2
A_{total}	Total heat exchange area, m^2
A_{tube}	Tube area, m^2
A_{ij}	Integration of area, m^2
C	Specific heat capacity of water, J kg^{-1} K^{-1}
C_p	Specific heat capacity of air, J kg^{-1} K^{-1}
h	Overall heat transfer coefficient, Wm^{-2} K^{-1}
$\dot{m}$	Water mass flow rate, kg s^{-1}
ΔQ	Total heat transfer, J
Q	Normal state heat transfer rate, W
Q_{ideal}	Ideal state heat transfer rate, W
T_{in}	Inlet temperature of air, K
T_{out}	Outlet temperature of air, K
t_{in}	Inlet temperature of water, K
t_{out}	Outlet temperature of water, K
ΔT_{ln}	Logarithmic temperature difference, K
u_{in}	Average air flow velocity, ms^{-1}

Greek symbols

ρ	Air density, kg m^{-3}

✉ Zhen Hu
1713086187@qq.com

Yongliang Zhang
zhyoliang@163.com

Hongwei Mu
muhongwei@qut.end.cn

Xilong Zhang
zhangxilong@qut.end.cn

Shouqing Lu
lushouqing20@163.com

Qinglei Tan
tqlfighting@163.com

Bing Shao
upcshaobing@163.com

[1] School of Mechanical & Automotive Engineering, Qingdao University of Technology, Qingdao 266033, China

Published online: 05 September 2024

Introduction

With decades of mineral mining operations, surface mineral resources in major mining areas are starting to become scarce, prompting a shift toward deeper sources. However, mining at greater depths introduces challenges such as longer, deeper, and more intricate mine tunnels [1, 2]. The increased heat generation in the surrounding rock makes ventilation and heat dissipation more challenging, leading to a prominent heat damage issue in mines. This, in turn, results in a higher incidence of occupational diseases and safety accidents [3–5].

In addressing the heat damage problem, some researchers have suggested employing small cooling fans to reduce temperatures in key underground areas. This approach involves creating designated cooling zones to establish microenvironments with comfortable temperatures. Notably, this method boasts a straightforward structure, easy installation and implementation, and proves to be cost-effective and energy-efficient [6, 7]. The cooling heat exchanger, typically installed at the end of the fan, commonly employs a finned-tube circulation tube as its core cooling structure. This configuration offers advantages such as a compact size and high cooling efficiency [8–12]. However, the fin-and-tube heat exchanger (FTHXs) often encounters challenges related to the complexity of its cooling medium flow path and uneven fluid flow. These issues serve as constraints that hinder the potential enhancement of its heat transfer performance. Consequently, there is a current emphasis on addressing and optimizing the flow path structure of heat exchangers [13–16].

The optimization of the flow path in finned-tube heat exchangers has been a subject of extensive research. Zhang [17] developed the Generalized Simulation Platform for Refrigeration and Air Conditioning Systems (GREATLAB) in 2010. This simulation platform offers robust technical support for simulating, optimizing, and controlling heat pump and air conditioning units. Given the similarities between mine fan heat exchangers and air conditioning systems, this study draws inspiration from the principles of GREATLAB and its related literature.

Mario Petrovic et al. [18] introduced topological concepts for optimizing the local structure of fins in a parallel plate heat exchanger using a genetic algorithm. Unlike the symmetrical and homogeneous configuration of conventional fin structures, the final optimized structure exhibits a slightly different shape for each row of fins within the airflow path. Validation experiments using 3D printed models demonstrated that the optimized structure outperformed the conventional counterpart.

In a study by Ishaque et al. [19], a dual-mode optimization algorithm was employed to enhance the performance of the heat exchanger's cooling water flow path, resulting in a performance improvement of up to 9.64%. The authors considered the inhomogeneity of air velocity in the heat exchanger and introduced knowledge-based (KBCM) and arrangement (PBCM) calculation modules to determine the optimal number of tubes and their arrangement while minimizing computational costs. The study utilized a program to align the flow paths, combining accurate heat transfer calculations for all paths with high precision but requiring substantial computational effort.

Domanski et al. [20] explored the application of an intelligent optimization module (ISHED) in optimizing refrigerant circuits. Their findings indicated that an intelligent automatic optimization system can yield comparable or even superior results compared to manual optimization [21].

Genetic algorithms provide a means to establish optimization objectives within a program, granting the algorithm a degree of autonomy, automating certain aspects of the optimization process, thereby saving time in the flow path optimization [22]. Jiang [23] employed genetic algorithms by transforming the heat exchanger tubes and their connections into a matrix and its units, optimizing their flow paths through this approach.

Wu et al. [24] utilized genetic algorithms to optimize refrigerant flow paths in heat exchangers, aiming for maximum heat transfer with the minimum pipe length as the objective. The optimized structure achieved a remarkable up to 40% reduction in the length of the heat exchanger header pipe and up to a 7.8% improvement in heat transfer performance. However, the iterated heat exchanger structure generated by the algorithm, while theoretically offering higher heat transfer performance, encountered challenges such as cross and far-span connections, thereby increasing manufacturing difficulty and costs. Human-imposed constraints and rules are often required to mitigate these issues.

In recent years, the rapid development of machine learning and artificial intelligence has opened up new possibilities. Large language models of artificial intelligence have demonstrated their potential, and these computational approaches can also be applied to the optimization design of heat exchangers [25, 26]. Mohammad Ghalandari et al. [27] mentioned that the application of various artificial intelligence techniques can be used to model and predict the performance of different heat exchangers. For example, these techniques can predict heat exchanger performance, processing costs, and fouling conditions during operation. The authors discussed the applications of different types of heat exchangers, such as shell-and-tube heat exchangers, which are suitable for high-pressure environments and offer design flexibility and low maintenance costs. Plate-type heat exchangers have a more compact structure and are suitable for low-pressure operating environments compared to shell-and-tube heat exchangers. Maunu Kuosa et al. [28]

conducted a study on the application of plate heat exchangers in the field of district energy-efficient heating. In plate heat exchangers, the two fluids involved in heat exchange are both waters. Low-temperature water and high-temperature water exchange heat through alternating heat exchange plates. The authors proposed a novel mass flow control model that improves the heat transfer performance of the plate heat exchanger while reducing pressure loss.

In conclusion, the majority of studies on flow path optimization for heat exchangers have focused on air conditioning systems, with relatively fewer investigations into the optimization of flow paths for small cooling heat exchangers in mining applications. The finite unit method, which discretizes the continuous structure to facilitate optimal design for specific micro-units, has been commonly employed in this research domain.

In this work, a mining fan heat exchanger unit optimization method based on previous research is proposed. This method involves the segmentation of the heat exchanger into units, the measurement and calculation of the working characteristics of individual units, and the utilization of a software program. By setting optimization objectives and instructing the program, the heat exchanger units are arranged and combined to find the optimal structure for the flow path arrangement. The ultimate aim is to enhance efficiency and address heat damage issues in mines, providing valuable technical support for mining operations. This approach utilizes the concept of finite element analysis to simplify the optimization of the heat exchanger flow path. This method is relatively novel, with few similar studies available in the existing literature.

Theoretical analysis

At the termination point of the mining fan, hot air is conveyed to the heat exchanger, facilitating heat exchange with the cooling water within. Assuming no consideration for the phase change of water vapor in the air, the energy exchanged per unit time can be expressed using Newton's law of cooling [29]:

$$\Delta Q = A_{\mathrm{f}} \cdot u_{\mathrm{in}} \cdot \rho \cdot C_{\mathrm{p}}(T_{\mathrm{in}} - T_{\mathrm{out}}) = \dot{m} \cdot C \cdot (t_{\mathrm{out}} - t_{\mathrm{in}}) \quad (1)$$

where ΔQ is the total heat transfer, A_{f} is the airflow inlet area, u_{in} is the average air flow velocity, ρ is the air density, C_{p} is the air constant pressure specific heat capacity, $\dot{m}$ is the mass flow of water, C is the specific heat capacity of water, T_{in}, t_{in} is the inlet temperature of air and water, respectively, T_{out}, t_{out} is the outlet temperature of air and water, respectively.

This method operates on the principle of calculating the temperature and flow rate differences before and after fluid heat exchange per unit time, enabling the determination of the heat exchange quantity. Given the relatively small change in the flow rates of air and cooling water coupled with significant temperature differences, this mathematical model can be conceptualized as a system. In this system, the initial temperature of the fluid serves as the input at one end, and the temperature of the fluid after heat exchange serves as the output at the other end [5]. Refer to Fig. 1 for a visual representation of this system.

In the context of a quadratic equation, obtaining solutions for two unknowns necessitates a minimum of two mathematical relationships. Similarly, in the domain of heat exchangers, the heat exchange volume can be determined through the fin efficiency and the heat transfer coefficient [30]. This relationship can be expressed as follows:

$$\Delta Q = A_{\mathrm{total}} \cdot \Delta T_{\mathrm{ln}} \cdot h \quad (2)$$

where A_{total} is the effective area of the fins [31], which can be expressed as:

$$A_{\mathrm{total}} = A_{\mathrm{tube}} + A_{\mathrm{fin}} \cdot \eta \quad (3)$$

where η is the fin efficiency, which is derived from simulation experiments and is calculated by assuming that the temperature of the fins is the same as the water pipe and does not change, and deriving the heat exchange in that case and

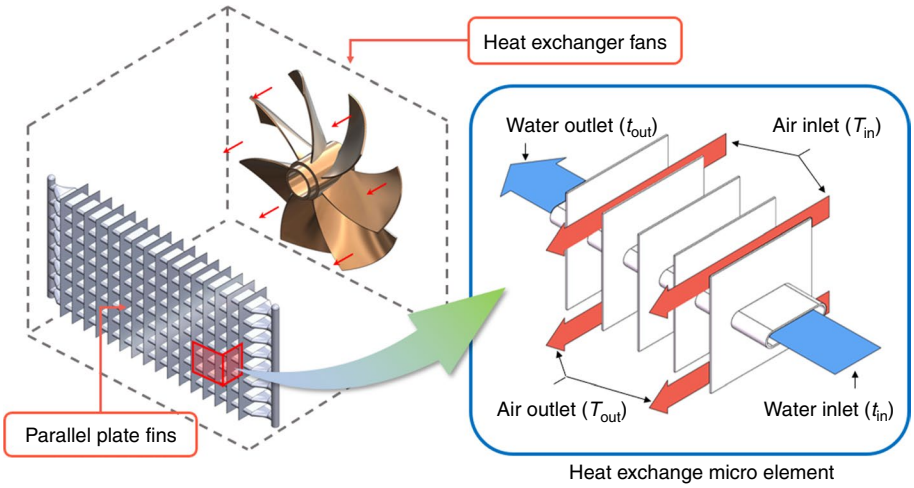

Fig. 1 Schematic diagram of micro-unit heat transfer characteristics

comparing it with the heat exchange of the fins for normal heat dissipation. It can be expressed as:

$$\eta = Q/Q_{\text{ideal}} \tag{4}$$

where Q is the heat exchange per unit time of the normal fin; Q_{ideal} represents the ideal maximum heat transfer rate per unit time, which is obtained through numerical simulation by artificially adjusting the fins to be isothermal with the water pipes. The mathematical expressions for Q and Q_{ideal} are as follows [29, 32]:

$$Q = \sum A_{ij}(T_f - T_{ij})h_{ij} \tag{5}$$

$$Q_{\text{ideal}} = \sum A_{ij}(T_f - T_{\text{tube}})h_{ij} \tag{6}$$

Equations 5 and 6 express the calculation methods for the heat exchange rate, T_f represents the air temperature. The difference between the two equations is that T_{ij} represents the temperature of the fin, which varies with changes in ij during the integration process, while T_{tube} is the fin temperature, but its value is equal to the temperature of the water pipe and remains constant. In the experiments conducted in this paper, the value of Q_{ideal} is derived from simulation experiments.

$\Delta T_{\ln}$ is the logarithmic temperature difference, and its calculation can be expressed as:

$$\Delta T_{\ln} = \frac{(T_{\text{in}} - t_{\text{out}}) - (T_{\text{out}} - t_{\text{in}})}{\ln \frac{T_{\text{in}} - t_{\text{out}}}{T_{\text{out}} - t_{\text{in}}}} \tag{7}$$

The heat transfer coefficient (h) signifies the effectiveness of overall heat transfer performance and is influenced by the shape and material of the heat exchanger, as well as the flow rate and flow state of the fluid. In a given model, when the aforementioned parameters remain constant, the heat transfer coefficient tends to be relatively fixed. Experimental investigations for different heat exchangers allow the determination of heat transfer coefficients [27].

If the inlet temperatures of air and water are considered as the primary characteristics of heat transfer, the heat transfer coefficient (h) can be expressed as a function of these characteristics. The values of the heat transfer coefficient for various cases are determined through simulation or experimentation and are often fitted using polynomials to establish a functional relationship. This relationship can be expressed as:

$$h = A_1 + A_2 T_{\text{in}} + A_3 t_{\text{in}} + A_4 T_{\text{in}} t_{\text{in}} + A_5 T_{\text{in}}^2 + A_6 t_{\text{in}}^2 \tag{8}$$

In the second method of calculating ΔQ, all parameters can be obtained either directly or indirectly, with the exception of the inlet and outlet temperatures of air and water. Given that the two calculation methods are founded on different physical principles, they can be amalgamated into a system of binary equations. In this system, the independent variables are the inlet temperatures of air and water (T_{in}, t_{in}), while the dependent variables are the outlet temperatures of air and water (T_{out}, t_{out}). This relationship can be expressed as:

$$\begin{cases} A_f \cdot u_{\text{in}} \rho \cdot C_p (T_{\text{in}} - T_{\text{out}}) = \dot{m} \cdot C \cdot (t_{\text{out}} - t_{\text{in}}) \\ A_f \cdot u_{\text{in}} \cdot \rho \cdot C_p (T_{\text{in}} - T_{\text{out}}) = A_{\text{total}} \cdot \Delta T_{\ln} \cdot h \\ h = f(T_{\text{in}}, t_{\text{in}}) \\ \Delta T_{\ln} = \frac{(T_{\text{in}} - t_{\text{out}}) - (T_{\text{out}} - t_{\text{in}})}{\ln \frac{T_{\text{in}} - t_{\text{out}}}{T_{\text{out}} - t_{\text{in}}}} \end{cases} \tag{9}$$

Physical model and numerical method

Heat exchanger flow path micro-unit optimization method introduction

In the cooling heat exchanger situated at the end of the mine fan, the arrangement of cooling water pipes within the internal space significantly influences the heat exchanger's efficiency. However, the three-dimensional spatial arrangement of cooling water pipes is inherently complex, making the identification of the optimal structure challenging through manual methods. To address this challenge, this paper introduces a micro-unit optimization method for the heat exchanger flow path. The method involves partitioning the fin-and-tube heat exchanger into several independent micro-units [33], interconnected as depicted in Fig. 2.

In Fig. 2, the cooling water sequentially passes through finned tube micro units B, A, C, and D. Consequently, the water flow outlet temperature from the preceding unit serves as the water flow inlet temperature for the subsequent finned tube unit. Additionally, considering the air flow direction, finned tube unit A is positioned upwind of unit B. The air flow outlet temperature from unit A can thus be used as the air flow inlet temperature for unit B.

Viewing the heat exchanger comprehensively, it can be segmented into distinct unit sections. The relationship between a unit and its neighboring units can be approximated as temperature iterations in both the air flow and water flow directions. This method, particularly effective for intricate heat exchanger flow structures, allows for small-scale experiments to fine-tune mathematical model parameters before applying them to more complex heat exchangers. By simplifying the computational process, this method ensures accuracy while reducing experimental costs and facilitating the application of computer algorithms for adjusting the heat exchanger flow path.

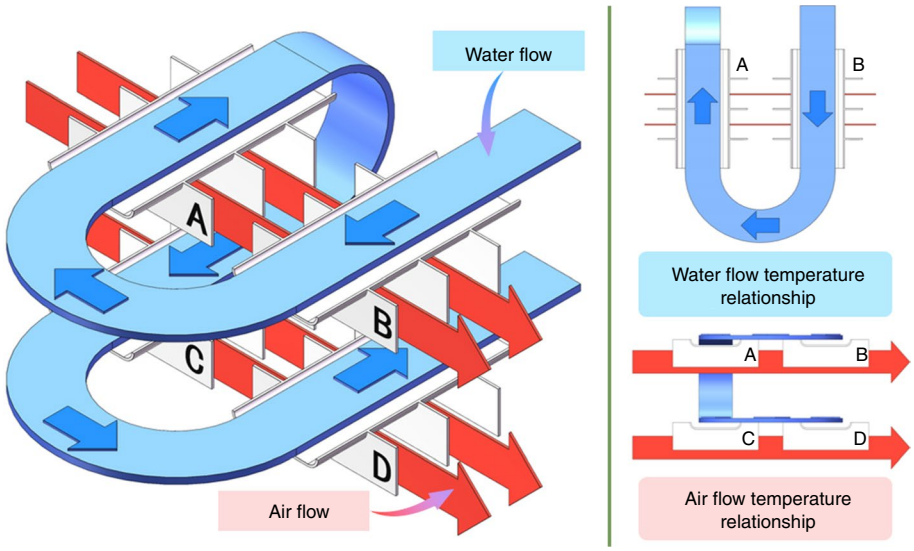

Fig. 2 Schematic diagram of heat exchange micro-unit temperature relationship

Heat exchanger flow path unitization optimization method mathematical model

Dividing the heat exchanger into several units introduces four key parameters within a given unit: the inlet temperature of air and water (T_{in}, t_{in}), and the outlet temperature of air and water (T_{out}, t_{out}). If a heat exchanger unit is denoted as A, its key parameters can be represented as $T_{A\,in}$. To integrate these parameters with the previously discussed theory, the circulating heat exchange process of air and water inside the heat exchanger can be articulated using mathematical language.

Referring to Fig. 2 for the heat exchanger, there are four heat exchange units (A, B, C, D), and they can be expressed in terms of a mathematical model as:

$$\begin{cases} A_f \cdot u_{in} \cdot \rho \cdot C_p(T_{in} - T_{out}) = \dot{Q} \cdot \rho \cdot C \cdot \left(t_{out} - t_{in}\right) \\ A_f \cdot u_{in} \cdot \rho \cdot C_p(T_{in} - T_{out}) = A_{total} \cdot \Delta T_{ln} \cdot h \\ \Delta T_{ln} = \frac{(T_{in} - t_{out}) - (T_{out} - t_{in})}{\ln \frac{T_{in} - t_{out}}{T_{out} - t_{in}}} \\ h = f\left(T_{in}, t_{in}\right) \\ T_{A\,out} = T_{B\,in} \\ T_{C\,out} = T_{D\,in} \\ t_{B\,out} = t_{A\,in} \\ t_{A\,out} = t_{C\,in} \\ t_{C\,out} = t_{D\,in} \end{cases} \tag{10}$$

Heat transfer coefficient solution

As mentioned earlier, h represents the overall heat transfer coefficient, reflecting the efficiency of heat transfer performance. Its value is interconnected with the shape and material of the heat exchanger, as well as the flow rate and flow state of the fluid [6]. Within the same model, the heat transfer coefficient remains relatively constant when the above parameters are held steady. Experimental determination is typically required to find the heat transfer coefficients for different heat exchangers.

The simple model employed for the simulation experiments, along with its primary parameters and boundary conditions, is illustrated in Fig. 3.

By modeling the micro-elements using SolidWorks, separate models were created for the water pipes, fins, and air domain. Then, COMSOL multiphysics was used for meshing and simulation. The inlet was set as a velocity inlet, and the outlet was set as a pressure outlet, with backflow suppressed. Except for the heat exchange boundaries and inlets/outlets, all other boundary conditions were set to thermal insulation.

A series of orthogonal experiments were devised to determine the heat transfer coefficient h of the heat exchanger. This involved substituting various air inlet temperatures and water inlet temperatures and creating a contour plot of the heat transfer coefficient. The solution results and schematic diagram are presented in Fig. 4.

Utilizing the heat transfer coefficients obtained from different temperature combinations, a function is fitted employing the least squares method. In this fitting process, the temperatures of air and water serve as dependent variables. The resulting heat transfer coefficient function within the given interval is derived as:

$$\begin{aligned} h =& 140.16 + (-0.57)T_{in} + 0.59t_{in} + (-5.81^{-4})T_{in}t_{in} \\ &+ 6.66^{-6}T_{in}^2 + (-5.98^{-6})t_{in}^2 \end{aligned} \tag{11}$$

The heat transfer coefficient function symbolizes the heat transfer performance of this specific heat transfer micro-unit

under the specified boundary conditions. In the event of alterations to the boundary conditions or the replacement of the heat transfer micro-unit, it becomes necessary to recalculate the heat transfer coefficient function.

Heat exchanger flow path unitization optimization method validation

Simulation Validation

To assess the feasibility and accuracy of the micro-unit optimization method for heat exchangers, simulation software was utilized. Experimental methods and assumptions

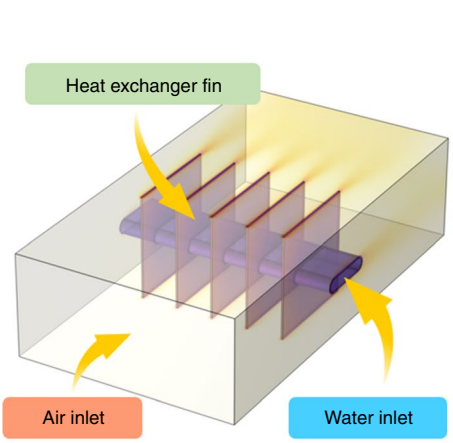

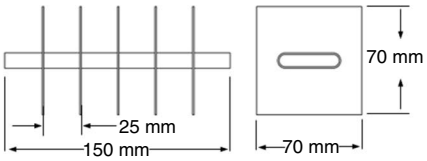

Boundary parameter settings			
Parameter	Value	Parameter	Value
Airflow temperature	303.15 K	Fin thickness	0.1 mm
Water flow temperature	283.15 K	Total heat exchange area	5.88e–2 m²
Airflow velocity	3 m/s	Fin heat exhange efficiency	78.47%
Water flow velocity	1 m/s	Water flow cross-sectional area	3.04e–4 m²

The inlet is set as a velocity inlet and the outlet is set as a pressure outlet. the boundary conditions are thermally insulated except for the heat transfer boundary and the inlet and outlet.

Fig. 3 Micro-unit model used to solve for the heat transfer coefficient

Heat transfer coefficient at different parameters *h*		Air temperature/K				
		303.15	308.15	313.15	318.15	328.15
Water temperature /K	283.15	0.2338	0.2313	0.2290	0.2268	0.2246
	286.15	0.2317	0.2294	0.2271	0.2249	0.2227
	289.15	0.2295	0.2273	0.2250	0.2228	0.2207
	292.15	0.2272	0.2250	0.2228	0.2207	0.2186
	295.15	0.2245	0.2226	0.2205	0.2184	0.2164

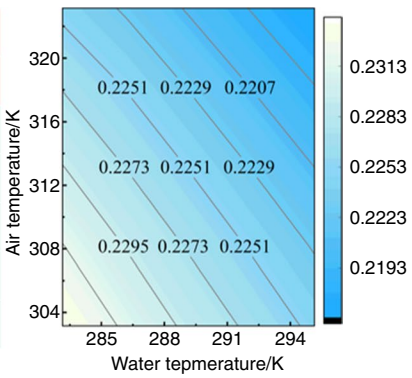

Fig. 4 Distribution of heat transfer coefficient

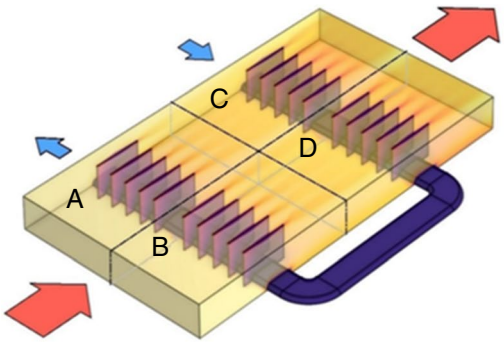

Boundary parameter settings			
Parameter	Value	Parameter	Value
Airflow temperature	323.15 K	Fin thickness	0.1 mm
Water flow temperature	286.15 K	Total heat exchange area	0.235 m²
Airflow velocity	3 m/s	Number of microelements	4
Water flow velocity	1 m/s	Water flow cross-sectional area	3.04e–4 m²

Fig. 5 Model used to validate numerical simulations

used, same as in the previous subsection. Verification of this approach took place under the primary boundary conditions depicted in Fig. 5.

The validation experiments for simulation were performed using a total of four heat transfer micro-units. These were solved using both software numerical simulation and the micro-units method mathematical calculation. The experiments employed identical boundary conditions, and detection points were set along the air and water flow paths. The specific locations of the two solution models and their corresponding detection points are illustrated in Fig. 6.

Temperature detection points are strategically positioned in both the micro-unit method solution model and the numerical simulation model. The measured temperature data from these points are then graphically represented, as depicted in Fig. 7.

The results obtained from the micro-unit method and numerical simulation indicate that the micro-unit method yields an average air outlet temperature of 316.55 K, whereas the numerical simulation results show 316.98 K, resulting in a difference of 0.43 K. For the average water outlet temperature, the micro-unit method provides 287.14 K, while the numerical simulation results in 287.05 K, resulting in a difference of 0.90 K. The temperature changes in the process exhibit a relatively small discrepancy between the two methods, and the temperature difference between the calculation methods is lower than the overall temperature difference at the outlet throughout the entire process. In summary, the temperature prediction and simulation difference for a basic heat exchanger comprised of four micro-units is minimal between the micro-unit method and numerical simulation. This can be attributed to the incorporation of crucial parameters, such as heat transfer coefficient and effective heat transfer area, from the numerical simulation into the micro-unit method. Consequently, the temperature change parameters exhibit similarities between the two methods.

In conclusion, the heat exchanger micro-unit optimization method represents a mathematical calculation approach grounded in numerical simulation. When applied to the flow path arrangement of the heat exchanger, it streamlines the computation for adjusting the heat exchanger flow path and contributes to enhancing the efficiency of this process. Additionally, the heat exchanger micro-unit optimization method

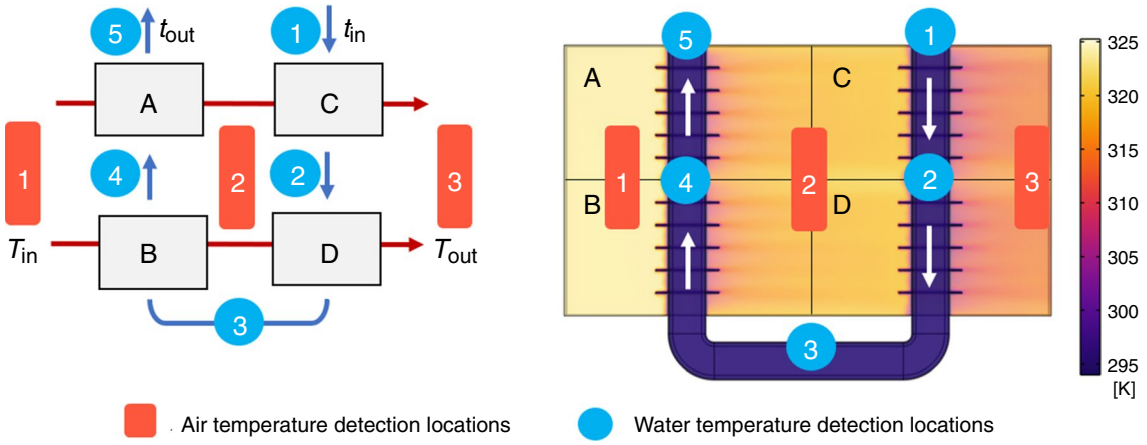

Fig. 6 Micro-unit method solution model and numerical simulation model

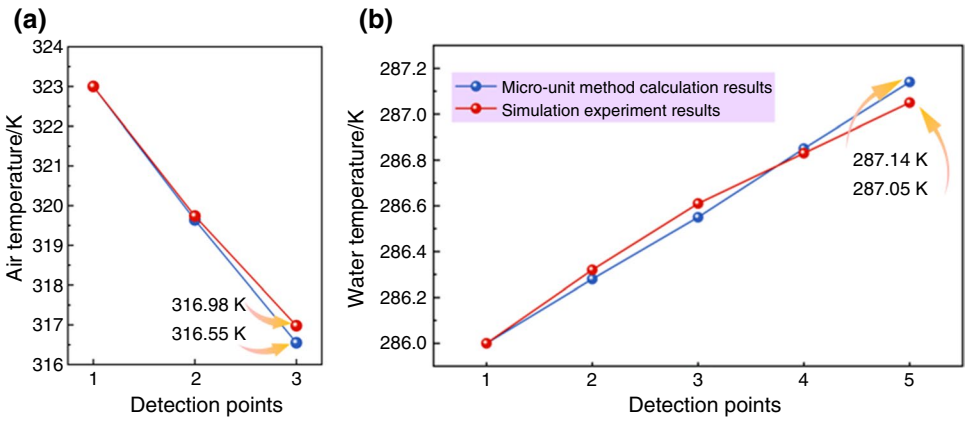

Fig. 7 Temperature at the detection point for the micro-unit method solved model and numerical simulation model

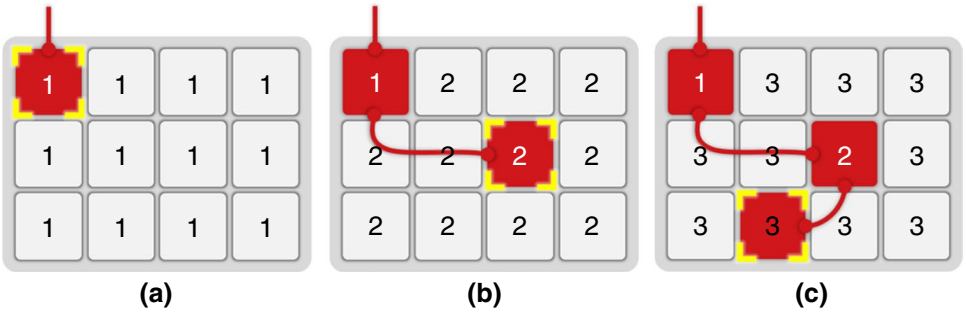

Fig. 8 Schematic diagram of heat exchanger division unit

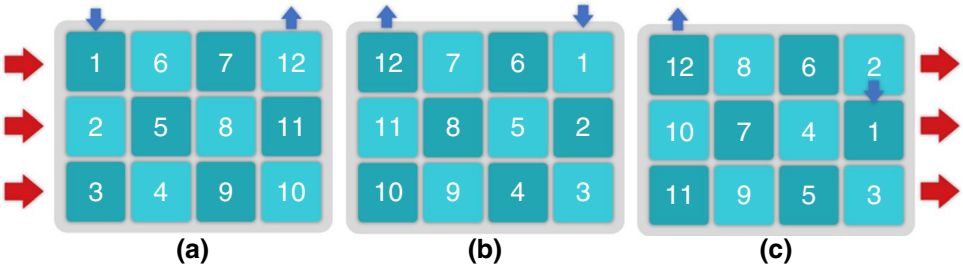

Fig. 9 Schematic diagram of representative flow path structure

can extract the heat transfer characteristics of the physical heat exchanger. Both the micro-unit optimization method based on physical heat transfer characteristics and the micro-unit method based on numerical simulation share the same underlying principle. Combining the micro-unit method, numerical simulation, and actual experiments can further enhance the efficiency of optimizing the heat exchanger flow path arrangement.

Heat transfer micro-units randomly arranged

The randomized arrangement of heat exchanger microcells is achieved through the utilization of software code. This subsection employs an example featuring 12 heat exchanger microcells, illustrated in Fig. 8.

In Fig. 8, the heat exchanger plumbing must identify the first heat exchanger micro-unit to serve as the entry point for the water flow and act as the inlet for the heat exchanger. Among the 12 heat exchanger micro-units depicted in Fig. 9, the 1st micro-unit can be chosen from 12 options. After determining the first heat exchanger micro-unit, the 2nd micro-unit needs to be selected from the remaining 11, resulting in (12 * 11) 132 possible combinations. This process continues, with the 3rd heat exchanger micro-unit having 10 choices, and so forth, until all 12 heat exchanger micro-units are selected, generating a total of (12!) 479,001,600 combinations. Many of these combinations are duplicates or hold no meaningful permutations, such as symmetrical ordering and confusing, unrealistic sequences. To exclude these irrelevant calculations, it is essential to sift through all the combinations.

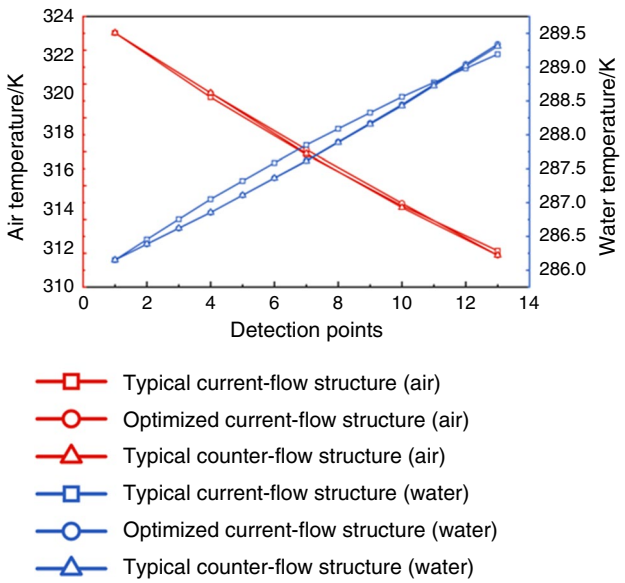

Fig. 10 Process temperature for different flow path structures

Analysis and discussion

In Fig. 9a, the typical current-flow structure is illustrated; Fig. 9b depicts the typical counter-flow structure, while Fig. 9c showcases the optimized counter-flow structure obtained through program solutions. The cooling water path is equipped with 12 detection points, each capturing the water flow temperature at its respective location. Additionally, 4 detection points are strategically placed along the wind flow path, where the average temperature of the wind flow is detected at the outlet of the heat exchange layer

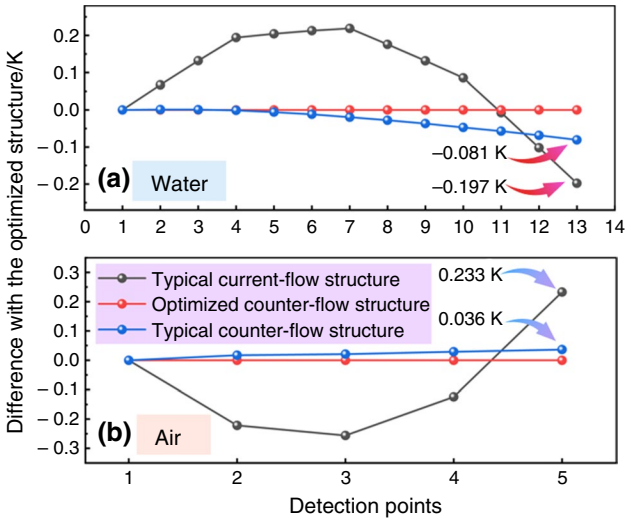

Fig. 11 Temperature difference between typical current-flow and counter-flow structures and optimized structures

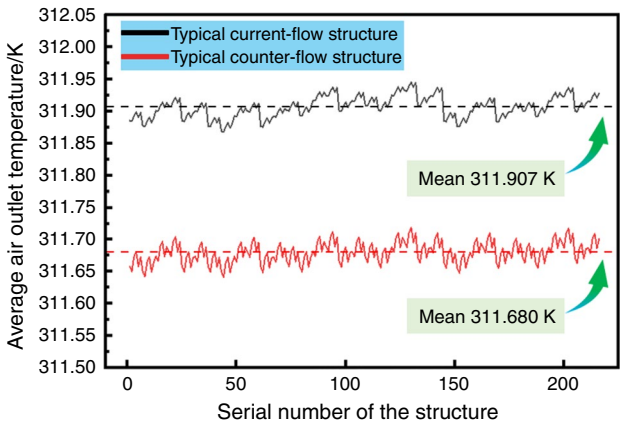

Fig. 12 Comparison of outlet temperature of downstream and counterflow structure

composed of heat exchange micro-units at each point. The resulting temperature curves are presented in Fig. 10.

To assess the process temperature difference among the three structures, the temperature variance between the typical current-flow and counter-flow structures and the optimized counter-flow structure at each detection point is graphically represented in line graphs. Figure 11 illustrates the air and water flow temperature difference graphs, respectively.

Upon examining Fig. 11a, it becomes evident that during air temperature changes, as the air and water flow in the same direction in the current-flow structure, the air is initially exposed to the colder water flow. This results in a faster temperature reduction in the early stage. However, the temperature difference between air and water diminishes in the later stages, causing a decrease in heat transfer rate. Ultimately, this leads to a higher air outlet temperature compared to the other two flow structures and a less effective overall heat transfer. On the other hand, both the counter-flow structure and the optimized counter-flow structure, with water flowing in the opposite direction to the air, exhibit a larger average heat transfer temperature difference. Consequently, the final heat transfer effect is superior to that of the current-flow structure.

Analyzing Fig. 11b reveals that the water flow in the current-flow structure experiences a rapid temperature increase during the initial heat exchange process, followed by a gradual decrease in speed, mirroring the air temperature change in Fig. 11a). At the outlet of the water stream in the heat exchanger, the end stream temperatures are comparable for all three flow structures.

Comparatively, the optimized structure, in contrast to the typical counter-flow structure, undergoes a similar heat transfer process, resulting in a temperature difference curve that follows a similar trend. However, the optimized structure exhibits a higher average water flow temperature and a lower average air temperature, contributing to a more effective heat transfer. This suggests that a more rational flow path arrangement can yield improved heat transfer efficiency.

Within the flow path optimization algorithm, certain unique flow paths with distinct characteristics are generated. Resembling Fig. 9a, these current-flow structures exclusively select the first layer of heat transfer micro-units as the inlet. After traversing all the micro-units in the first layer, they then select the second layer of heat transfer micro-units as the path. All such structures are collectively referred to as current-flow structures. Consequently, a total of 216 types each of down-flow and counter-flow structures are generated. The air outlet temperatures for all these structures are compiled into a statistical graph, as depicted in Fig. 12.

Upon analyzing Fig. 12, it becomes evident that, across all counterflow structures, the air outlet temperature is lower than that of the downflow structure. This suggests a more efficient heat transfer for the counterflow structure. The average air outlet temperature for the counter-flow structure is 313.680 K, which is lower than the 313.907 K of the current-flow structure. This implies that the counter-flow structure should be prioritized in the design of the heat exchanger flow path, as it offers superior heat transfer efficiency.

Upon analyzing Fig. 12, it becomes evident that, across all counterflow structures, the air outlet temperature is lower than that of the downflow structure. This suggests a more efficient heat transfer for the counterflow structure. The average air outlet temperature for the counter-flow structure is 313.680 K, which is lower than the 313.907 K of the current-flow structure. This implies that the counter-flow structure should be prioritized in the design of the heat exchanger flow path, as it offers superior heat transfer efficiency.

Conclusions

This paper studies mine heat exchangers and proposes a novel method for optimizing the flow path structure of heat exchangers. Through this method, the heat exchanger is divided into multiple micro-units, and numerical simulations are used to determine their heat transfer characteristics. Subsequently, a computer program is employed to comprehensively calculate the sequence of micro-units in the cooling water flow path. The research findings are summarized as follows:

1. A comprehensive arrangement of the 12 heat exchanger micro-units, as designed in this paper, resulted in the generation of a total of 479,001,600 flow path structures. Among these, the optimal structure exhibits an average air outlet temperature of 311.65 K. This value is lower than the air outlet temperatures of 311.88 K for a typical current-flow structure and 311.68 K for a typical counter-flow structure, demonstrating a superior heat transfer effect.
2. In the typical current-flow structure, the overall flow direction of the water stream aligns with the air flow direction. Although its air temperature experiences a faster initial drop during the heat transfer process compared to the counter-flow structure, the final outlet temperature is higher, indicating poorer heat transfer performance due to a lower temperature difference throughout the entire process. Notably, the heat transfer performance of all 216 counter-flow structures generated by the algorithm surpasses that of an equal number of current-flow structures. The average air outlet temperature for all counter-flow structures is 311.68 K, which is lower than the average air outlet temperature of 311.90 K for the current-flow structures. Therefore, in designing the heat exchanger flow path, optimizing the overall flow direction of the water to be opposite to the air flow direction as much as possible is recommended for achieving enhanced heat transfer results.
3. In this study, only 12 heat transfer micro-units are employed. In practical engineering heat exchangers, the number of micro-units post-division will be greater, resulting in a more intricate flow path structure. The substantial increase in calculation volume can pose challenges for the exhaustive algorithm. Additionally, this paper does not account for radiation and contact heat transfer between micro-units, contributing to a decrease in the algorithm's reliability.

Acknowledgements This research was supported by National Natural Science Foundation of China (52374209), Natural Science Foundation of Shandong Province (ZR2023ME012); Natural Science Foundation of Shandong Province (ZR2023QE080).

Author contributions Yongliang Zhang (First author) done funding acquisition, methodology, resources, investigation, conceptualization, and supervision. Zhen Hu (Corresponding author) contributed to conceptualization, software, writing—original draft, visualization, and writing—review and editing. Hongwei Mu done investigation, project administration, project administration. Xilong Zhang and Shouqing Lu contributed to conceptualization, methodology, and validation. Qinglei Tan done investigation, resources, and data curation. Bing Shao done supervision and project administration.

Data availability Data will be made available on request.

Declarations

Conflict of interest We have no conflicts of interest to declare.

References

1. Huang P, Huang W, Zhang Y, Tang S. Simulation study on sectional ventilation of long-distance high-temperature roadway in mine. Arab J Geosci. 2021;14(16):1674. https://doi.org/10.1007/s12517-021-07880-z.
2. Qu M, Zhang Y, Zhang X, Jia Y, Fu C, Yao Q, et al. A review: Analysis and development of heat–mass synergy theory. Energy Rep. 2022;8:14830–51. https://doi.org/10.1016/j.egyr.2022.11.021.
3. Zhongpeng X. Distribution law of high temperature mine's thermal environment parameters and study of heat damage's causes. Procedia Eng. 2012;43:588–93. https://doi.org/10.1016/j.proeng.2012.08.104.
4. Zhang Y, Huang P. Influence of mine shallow roadway on airflow temperature. Arab J Geosci. 2019;13(1):12. https://doi.org/10.1007/s12517-019-4934-7.
5. Xiaojie Y, Qiaoyun H, Jiewen P, Xiaowei S, Dinggui H, Chao L. Progress of heat-hazard treatment in deep mines. Min Sci Technol (China). 2011;21(2):295–9. https://doi.org/10.1016/j.mstc.2011.02.015.
6. Zhang Y, Zhang X, Li M, Liu Z. Research on heat transfer enhancement and flow characteristic of heat exchange surface in cosine style runner. Heat Mass Transf. 2019;55(11):3117–31. https://doi.org/10.1007/s00231-019-02647-5.
7. Zhang Y, Li M. Research on flow and heat transfer characteristics of heat transfer surface of trapezoidal duct. Heat Mass Transf. 2020;56(5):1475–86. https://doi.org/10.1007/s00231-019-02794-9.
8. Zhang X, Zhang Y, Liu Z, Liu J. Analysis of heat transfer and flow characteristics in typical cambered ducts. Int J Therm Sci. 2020;150: 106226. https://doi.org/10.1016/j.ijthermalsci.2019.106226.
9. Menéndez J, Ordóñez A, Álvarez R, Loredo J. Energy from closed mines: underground energy storage and geothermal applications. Renew Sustain Energy Rev. 2019;108:498–512. https://doi.org/10.1016/j.rser.2019.04.007.
10. Blecich P, Trp A, Lenić K. Thermal performance analysis of fin-and-tube heat exchangers operating with airflow nonuniformity. Int J Therm Sci. 2021;164: 106887. https://doi.org/10.1016/j.ijthermalsci.2021.106887.
11. Bhandari P, Prajapati YK. Thermal performance of open microchannel heat sink with variable pin fin height. Int J Therm Sci.

2021;159: 106609. https://doi.org/10.1016/j.ijthermalsci.2020.106609.
12. Okbaz A, Pınarbaşı A, Olcay AB. Experimental investigation of effect of different tube row-numbers, fin pitches and operating conditions on thermal and hydraulic performances of louvered and wavy finned heat exchangers. Int J Therm Sci. 2020;151: 106256. https://doi.org/10.1016/j.ijthermalsci.2019.106256.
13. Taler D. Mathematical modeling and control of plate fin and tube heat exchangers. Energy Convers Manage. 2015;96:452–62. https://doi.org/10.1016/j.enconman.2015.03.015.
14. Jin S, Wang X, Ma X, Wang Q. Study on the performance of small tube diameter R290 fin-tube evaporator. Procedia Eng. 2017;205:1578–83. https://doi.org/10.1016/j.proeng.2017.10.272.
15. Huang D, Jia J. Effect of refrigerant circuit arrangement of outdoor heat exchanger on performance of heat pump air conditioner. Hsi-An Chiao Tung Ta Hsueh/Journal of Xi'an Jiaotong University. 2010;44:33–7.
16. Sadeghianjahromi A, Wang C-C. Heat transfer enhancement in fin-and-tube heat exchangers—a review on different mechanisms. Renew Sustain Energy Rev. 2021;137: 110470. https://doi.org/10.1016/j.rser.2020.110470.
17. Sun L, Zhang C. System simulation and computational fluid dynamics based refrigerant circuitry optimization of a condenser. 2015; 43: 1390–1394. https://doi.org/10.11908/j.issn.0253-374x.2015.09.16
18. Petrovic M, Kenichiro F, Kenichi K. Numerical and experimental performance investigation of a heat exchanger designed using topologically optimized fins. SSRN Electron J. 2022. https://doi.org/10.1016/j.applthermaleng.2022.119232.
19. Ishaque S, Kim M-H. Refrigerant circuitry optimization of finned tube heat exchangers using a dual-mode intelligent search algorithm. Appl Therm Eng. 2022. https://doi.org/10.1016/j.applthermaleng.2022.118576.
20. Domanski PA, Yashar D. Optimization of finned-tube condensers using an intelligent system. Int J Refrig. 2007;30(3):482–8. https://doi.org/10.1016/j.ijrefrig.2006.08.013.
21. Cen J, Hu JP, Jiang F. An automatic refrigerant circuit generation method for finned-tube heat exchangers. Can J Chem Eng. 2018;96:2661–72. https://doi.org/10.1002/cjce.23150.
22. Lu B, Wu J, Liang Z, Liu C. Circuitry arrangement optimization for multi-tube phase change material heat exchanger using genetic algorithm coupled with numerical simulation. Energy Convers Manage. 2018;175:213–26. https://doi.org/10.1016/j.enconman.2018.08.108.
23. Jiang H, Aute V, Radermacher R. CoilDesigner: a general-purpose simulation and design tool for air-to-refrigerant heat exchangers. Int J Refrig. 2006;29(4):601–10. https://doi.org/10.1016/j.ijrefrig.2005.09.019.
24. Wu Z, Ding G, Wang K, Fukaya M. Application of a genetic algorithm to optimize the refrigerant circuit of fin-and-tube heat exchangers for maximum heat transfer or shortest tube. Int J Therm Sci. 2008;47(8):985–97. https://doi.org/10.1016/j.ijthermalsci.2007.08.005.
25. Celik N, Tasar B, Kapan S, Tanyildizi V. Performance optimization of a heat exchanger with coiled-wire turbulator insert by using various machine learning methods. Int J Therm Sci. 2023;192: 108439. https://doi.org/10.1016/j.ijthermalsci.2023.108439.
26. Kamsuwan C, Wang X, Piumsomboon P, Pratumwal Y, Otarawanna S, Chalermsinsuwan B. Artificial neural network prediction models for nanofluid properties and their applications with heat exchanger design and rating simulation. Int J Therm Sci. 2023;184: 107995. https://doi.org/10.1016/j.ijthermalsci.2022.107995.
27. Ghalandari M, Shahrestani MI, Maleki A, Shadloo MS, El Haj AM. Applications of intelligent methods in various types of heat exchangers: a review. J Therm Anal Calorim. 2021;145(4):1837–48. https://doi.org/10.1007/s10973-020-10425-3.
28. Kuosa M, Aalto M, El Haj AM, Mäkilä T, Lampinen M, Lahdelma R. Study of a district heating system with the ring network technology and plate heat exchangers in a consumer substation. Energy Build. 2014;80:276–89. https://doi.org/10.1016/j.enbuild.2014.05.016.
29. Su M, Gao Y, Zhao F, Liu Y, Li R, Li J. Numerical design of efficient slit fin surfaces with strips in different directions. Int J Therm Sci. 2023;192: 108421. https://doi.org/10.1016/j.ijthermalsci.2023.108421.
30. Tang LH, Zeng M, Wang QW. Experimental and numerical investigation on air-side performance of fin-and-tube heat exchangers with various fin patterns. Exp Thermal Fluid Sci. 2009;33(5):818–27. https://doi.org/10.1016/j.expthermflusci.2009.02.008.
31. Tao YB, He YL, Huang J, Wu ZG, Tao WQ. Numerical study of local heat transfer coefficient and fin efficiency of wavy fin-and-tube heat exchangers. Int J Therm Sci. 2007;46(8):768–78. https://doi.org/10.1016/j.ijthermalsci.2006.10.004.
32. Song K-W, Wang Y, Zhang Q, Wang L-B, Liu Y-J. Numerical study of the fin efficiency and a modified fin efficiency formula for flat tube bank fin heat exchanger. Int J Heat Mass Transf. 2011;54(11):2661–72. https://doi.org/10.1016/j.ijheatmasstransfer.2010.12.040.
33. Sadeghianjahromi A, Kheradmand S, Nemati H, Wang C-C. Optimization of the louver fin-and-tube heat exchangers-a parametric approach. J Enhanc Heat Transf. 2020;27:289–312. https://doi.org/10.1615/JEnhHeatTransf.2020033527.